nature physics

Article

https://doi.org/10.1038/s41567-024-02437-9

Search for charge non-conservation and Pauli exclusion principle violation with the MAJORANA DEMONSTRATOR

Received: 4 January 2023

Accepted: 8 February 2024

Published online: 11 April 2024

Check for updates

The MAJORANA Collaboration*

Charge conservation and the Pauli exclusion principle result from fundamental symmetries in the standard model of particle physics, and are typically taken as axiomatic. High-precision tests for small violations of these symmetries could point to new physics. Here we consider three models for violation of these processes, which would produce detectable ionization in the high-purity germanium detectors of the MAJORANA DEMONSTRATOR experiment. Using a 37.5 kg yr exposure, we report a lower limit on the electron mean lifetime, improving the previous best limit for the $e \rightarrow \nu_e\overline{\nu}_e\nu_e$ decay channel by more than an order of magnitude. We also present searches for two types of violation of the Pauli exclusion principle, setting limits on the probability of an electron to be found in a symmetric quantum state.

Searches for small violations of fundamental symmetries have driven modern experimental physics, from the discovery of parity non-conservation in beta decay[1], to tests demonstrating violations of Bell's inequality[2–4]. In this work we consider two well-validated principles of quantum mechanics, charge conservation and Pauli exclusion, which emerge from robust mathematical frameworks and are typically taken as axioms. Many models have been proposed which allow their violation by exotic mechanisms[5–12], and point to signs of new physics.

Large underground radiation detectors offer a unique environment to search for rare signals produced by such symmetry violations. The MAJORANA DEMONSTRATOR, a high-purity germanium (HPGe) array, has excellent energy resolution and ultra-low levels of radioactive backgrounds, and in addition to its primary search for neutrinoless double beta decay[13,14], it has been used to search for bosonic dark matter[15,16], fractionally charged particles[17], trinucleon decay[18] and signatures of quantum wavefunction collapse[19].

The DEMONSTRATOR consists of two separate modules of p-type point contact HPGe detectors, with 29.7 kg enriched in ^{76}Ge, and collected an ultimate exposure of 65 kg yr (ref. 14). From this primary dataset, an exposure of 37.5 kg yr of ^{enr}Ge data was selected for analysis of the 1–100 keV low-energy range. To produce the final spectrum, a series of analysis cuts are applied that remove events from electronics noise and energy-degraded surface events, while retaining bulk events above 20 keV with 92% efficiency[16]. The ^{enr}Ge detectors achieved background rates of 0.01 counts per keV kg d from 20–40 keV and 0.06 counts per keV kg d at 5 keV through use of highly radiopure materials, the deep underground location and careful control of the surface exposure time. In the energy spectrum, we observe a nearly flat continuum consisting of Compton scatter events between 20–100 keV, with visible contributions from ^{3}H, ^{55}Fe and ^{68}Ge below 20 keV.

In this work we present an experimental test of charge conservation, searching for the spontaneous disappearance of an electron to 'invisibles' (no photons), with the most favourable mode being to three neutrinos (ν), ($e \rightarrow \nu_e\overline{\nu}_e\nu_e$) (ref. 20). Our result for the mean lifetime of the electron is the best in more than two decades[21]. We then report limits on violations of the Pauli exclusion principle (PEP), which would also have a detectable ionization signature in our HPGe array. The 'forbidden' mechanisms considered are illustrated in Fig. 1.

Test of electric charge conservation

Conservation of electric charge arises from the unbroken local U(1) symmetry of the Standard Model, with the photon as its associated massless boson. Extremely small experimental upper limits on the photon mass are generally considered to be evidence of exact electric charge conservation. However, there are theoretical frameworks beyond the Standard Model which allow electric charge non-conservation, either

*A list of authors and their affiliations appears at the end of the paper. e-mail: inwookkim.physics@gmail.com; wisecg@uw.edu

https://doi.org/10.1038/s41567-024-02437-9

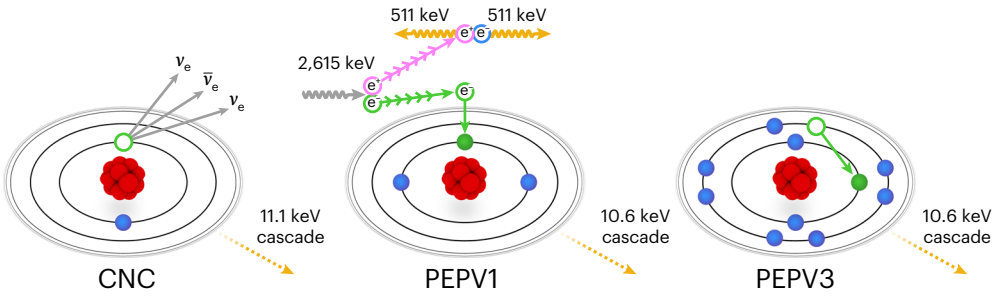

Fig. 1 | Three processes disallowed by quantum mechanics that would produce ionization in Ge atoms. A simplified view of the atom includes a nucleus (red) surrounded by the closest orbital electrons (blue) depicting their non-standard processes (green). Additional bound electrons are not illustrated for clarity. In each case, electrons from outer shells cascade to fill the vacancy, releasing energy as photons and Auger electrons. Left, charge non-conservation (CNC), with an electron decaying to three neutrinos, releasing 11.1 keV. Middle, PEP violation by a newly born electron produced by pair production from an incident 2,615 keV gamma (Type I) (PEPV1) releasing 10.6 keV along with two 511 keV gammas. (Pink and green lines denote the positron/electron paths.) Right, PEP violation where an electron descends to a fully occupied energy level (Type III) (PEPV3), releasing 10.6 keV.

by broken gauge symmetry or by hidden processes such as charge leakage into extra dimensions[22–25].

Violation of charge conservation implies that electrons, the lightest charged leptons, may have a finite lifetime. Hence, the conservation of electric charge can be tested by searching for the decay of electrons to chargeless particles with lighter mass, such as neutrinos and photons (γ). Experiments have set limits on the decay process ($e \to \nu_e\gamma$) by searching for a peak at 255.5 keV, with the best result from Borexino giving a mean lifetime $\tau_e > 6.6 \times 10^{28}$ yr (ref. 26). The electron may also decay without a photon to multiple neutrinos or other unknown chargeless beyond-Standard Model particles, often referred to as a 'disappearance' mode. Decay to three neutrinos ($e \to \nu_e\bar{\nu}_e\nu_e$) is considered the most favourable of these modes, being comprised of known particles which can balance angular momentum and conserve lepton number. In general, a search for electron disappearance would include effects from any 'invisible' mechanism, not only the three-neutrino mode. Disappearance mechanisms to date give lifetimes on the order of 10^{24} years[20], and we point out that if more than one decay mode is available for an electron, the channel with the shorter lifetime will be favoured.

Data from the low-background physics run of the DEMONSTRATOR can be used to search for decay of atomic electrons within the HPGe detectors. If a K-shell (ground state) electron in a Ge atom decays to neutrinos (or other invisibles), a hole is produced in the shell, and electrons in higher shells will cascade to fill it, emitting X-rays and Auger electrons until the full binding energy (11.1 keV) is released. This cascade occurs in a short timescale relative to the HPGe charge collection time, making the signature of this process a Gaussian peak in the spectrum at 11.1 keV.

In the region of interest, we perform an unbinned profile likelihood scan over the number of counts attributable to a rare signal. The excellent energy resolution allows discrimination from the nearby 10.37 keV X-ray line originating from ^{68}Ge electron capture decay, and the acceptance efficiency of the pulse shape analysis cuts is $(91 \pm 2)\%$ at 11.1 keV. The energy calibration provided by the primary neutrinoless double beta decay search analysis is validated by observation of the 10.37 keV line at the expected energy. The background function is a second-order Chebyshev polynomial, and nearby cosmogenic peaks are included in the model. This method is the same one used to search for peaked signatures in ref. 16 and further details are given in Methods.

Finding no statistically significant signal at 11.1 keV, as shown in Fig. 2, we report an upper limit on the event rate of $R = 0.00154$ counts per kg d to a 90% confidence level (CL). The corresponding limit on the mean lifetime $\tau_e = n_e/R$ is obtained from the upper limit on the decay rate per unit time R, the number density of Ge atoms, $N_{Ge} = 7.96 \times 10^{24}$ kg^{-1}, and two K-shell electrons for each Ge atom, $n_e = 2N_{Ge}$. We find a mean lifetime of $\tau_e(e \to \nu_e\bar{\nu}_e\nu_e) > 2.83 \times 10^{25}$ yr (90% CL), the most stringent

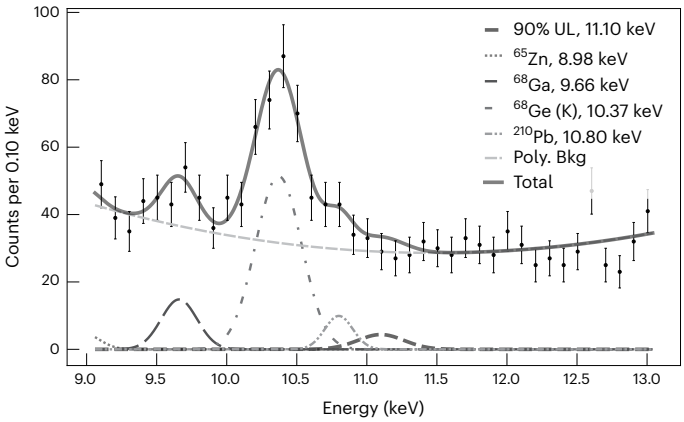

Fig. 2 | A charge non-conserving decay $e \to \nu_e\bar{\nu}_e\nu_e$ from a Ge K-shell electron would produce a peak at 11.1 keV. This peak is not observed in the 37.5 kg yr exposure collected, and an upper limit (UL) on the rate is set, $R = 0.00154$ counts (kg d)$^{-1}$ (90% CL). Data error bars are Poisson distributed, and the y axis is given in counts per 0.1 keV bin. Data are fit to a polynomial function (Poly. Bkg) with expected background lines from ^{65}Zn, ^{68}Ga, ^{68}Ge and ^{210}Pb. Additional details are given in Methods.

limit for this decay channel by a factor 11.8 over ref. 21, surpassing the previous best result published more than two decades ago.

Tests of Pauli exclusion principle violation

The PEP states that two identical fermions cannot occupy the same quantum state[27]. In modern quantum mechanics, it is understood to originate from the spin-statistics theorem, which describes the antisymmetric behaviour of fermions in quantum systems[28]. Many mechanisms of PEP violation have been proposed, making a direct comparison difficult[8,9,29–31]. Experimental tests of the PEP may set limits on the probability of two fermions to form a symmetric quantum state. In this work, that probability is taken to be a ratio of lifetimes between PEP-obeying (τ_{PEP}) and PEP-violating (τ_{PEPV}) atomic transitions of electrons, $\beta^2/2 \equiv \tau_{PEP}/\tau_{PEPV}$.

In this case, the transitions in which a model allows the PEP to be violated are determined by the initial symmetry state of the electron. The Messiah–Greenberg superselection rule[32] forbids electron transitions between states of differing symmetry, allowing only newly created electrons, or electrons already in a symmetric state, to make a transition to a symmetric final state. As electrons in symmetric states have not been observed, newly created ones provide the only model-independent test currently available. This constraint, however,

https://doi.org/10.1038/s41567-024-02437-9

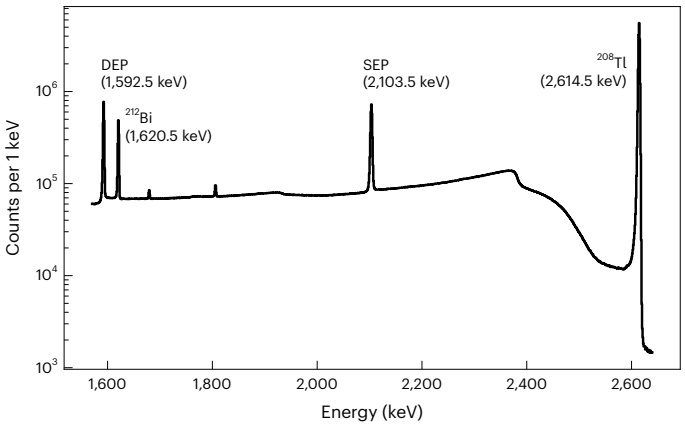

Fig. 3 | The combined ^{228}Th calibration spectrum from all active detectors in the MAJORANA DEMONSTRATOR. Prominent features include the full-energy peak from ^{208}Tl, the associated SEP and DEP, and a strong ^{212}Bi line near the DEP. Data was taken from 2015–2019, presented here in counts per 1 keV bin. Bin errors are Poisson distributed.

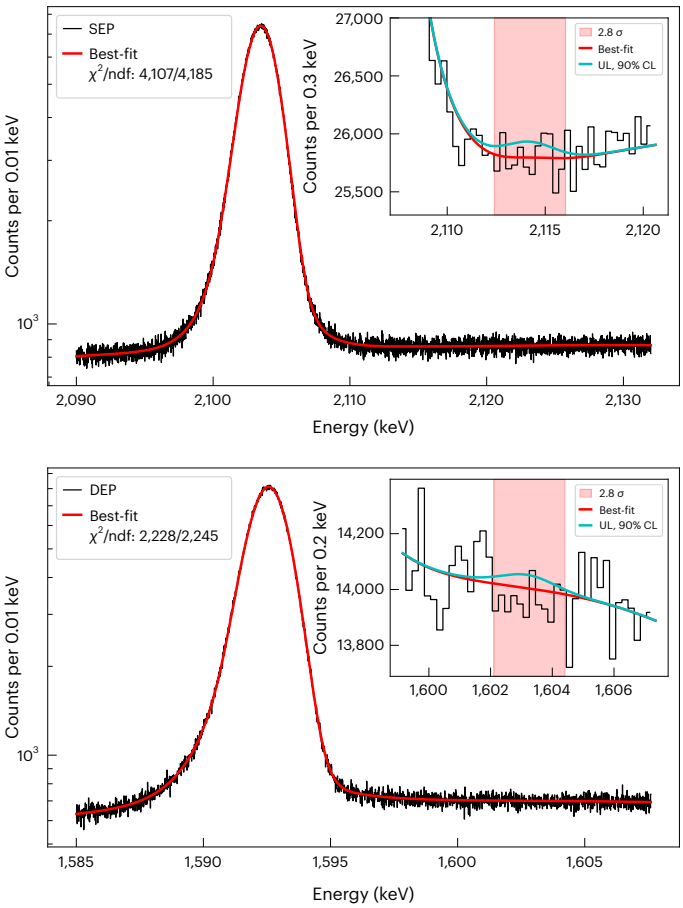

Fig. 4 | Searching for a violation of the Pauli exclusion principle via detection of an 'echo' peak. Fits to the SEP (top) and DEP (bottom) regions are shown, with the best-fit (red) and the 90% UL (cyan) in the inset. A 2.8-σ-wide region centred at the echo peak is shown for context. Bin errors are Poisson distributed, and the goodness-of-fit (χ^2/ndf) of the model is close to 1 in both cases. Additional details on the fits are given in Methods.

can be evaded by exotic physics such as the existence of extra dimensions or electron substructure[33,34]. More recently, it has been proposed that the violation of the spin-statistics theorem and hence PEP violation can emerge naturally from quantum gravity[35]. The paper by Elliott et al.[36] reviews the experimental and theoretical considerations. Following this framework, processes that can violate the PEP are classified into three categories:

- Type I interactions are between a system of fermions and a fermion that has not previously interacted with any other fermions. For example, a newly created electron from pair production has not yet established (anti-)symmetry with the surrounding atomic lattice, and a PEP-violating process is allowed by any model.
- Type II interactions are between a system of fermions and a fermion that has not previously interacted with that given system. For example, an extant electron introduced to an atomic lattice (for example, through an electric current) may have new PEP-violating interactions with that lattice, despite having already established antisymmetry with respect to distant systems.
- Type III interactions are between a system of fermions and a fermion within that given system. PEP violation in such interactions is only possible in models that avoid the Messiah–Greenberg superselection rule, as the PEP-violating fermion is already in an established symmetry state in its host system.

Each type of PEP violation can be tested experimentally with HPGe detectors, and tests of Types I and III are possible with the DEMONSTRATOR dataset. In this work, a Type I search is performed using ^{228}Th calibration data, and a Type III search is performed with the 37.5 kg yr low-energy background data. Type II searches have been done previously by the MAJORANA and VIP collaborations, using electrical currents through Pb and Cu as the transition sources[36–38]. We note that strong limits are available for both Type I and Type III processes based on searches for anomalous masses of primordial ^{5}Li (refs. 39,40) and for forbidden nuclear transitions in ^{12}C (ref. 41). However, both of these results consider transitions of strongly interacting nucleons in the potential generated by those same nucleons. The searches performed here with the DEMONSTRATOR involve purely atomic transitions of electrons in a potential that is dominated by the electromagnetic attraction of the (positive) nucleus, and are the most stringent available in such systems. As there is no comprehensive theoretical framework that accommodates PEP violation, we cannot directly compare our results here with the nuclear limits in refs. 39 and 41. Instead, we stress that it is valuable to perform such complementary tests in as wide a variety of qualitatively different systems as possible.

Type I PEP violation test with new electrons

The calibration system of the DEMONSTRATOR consisted of twin ^{228}Th line sources, periodically inserted into the system for weekly 60–90 min calibrations of each module, with several runs of longer duration for fine tuning of pulse shape analysis cuts. We utilize 40.43 days from the first detector module, and 21.38 days from the second module. The signature of Type I PEP violation in the MAJORANA calibration dataset can be observed (Fig. 1, middle scheme) from pair production events produced by 2614.5 keV gamma rays from the decay of ^{208}Tl in the ^{228}Th line source, which create electron–positron pairs in the detectors. The positron annihilation produces two 511 keV gamma rays, and one or both may escape the detector, creating single-escape peak (SEP) events at 2,103.5 keV and double-escape peak (DEP) events at 1,592.5 keV. If the PEP is violated, the pair-produced free electron may be captured by a Ge atom and transition to the already occupied K shell. In this process, the total binding energy of 10.6 keV is emitted, which is decreased from 11.1 keV as three electrons are present[36].

The full-energy peak at 2,614.5 keV contains a substantial contribution of ionization events with no pair production, which precludes its use in our search. The additional cascade produced by the PEP-violating capture to the K shell sums with the escape peak energy deposition, making the signature of the transition a peak 10.6 keV above the

Table 1 | Upper limits on the $\beta^2/2$ PEP-violating parameter from analysis of the SEP and DEP

	$\beta^2/2$ 90% CL	$\beta^2/2$ 99.7% CL
DEP	3.22×10^{-4}	8.32×10^{-4}
SEP	9.99×10^{-4}	1.57×10^{-3}
Combined	$\mathbf{3.69\times10^{-4}}$	7.79×10^{-4}

While the DEP result is more stringent (at 90% CL), the same underlying mechanism applies to both escape peaks, and we report the combined result from both escape peaks as the primary result (bold text).

SEP and DEP. The best prior limit for this process is $\beta^2/2 < 1.4\times10^{-3}$ (99.7% CL)[36] achieved by using a single HPGe detector and ^{232}Th source, with 3 weeks of runtime. Our calibration runtime and active detector mass are both significantly larger, taken over the multiyear run of the DEMONSTRATOR. The spectrum used for our Type I search is shown in Fig. 3, with standard data cleaning and quality cuts applied[42].

To search the regions above the DEP and SEP for a PEP-violating ('echo') peak, we perform a standard extended binned likelihood fit, using the precision peak-shape function given in ref. 43. Fit results for both regions are shown in Fig. 4. In addition to the main Gaussian term, it includes contributions modifying the high- and low-energy tails of the escape peaks, with a Legendre polynomial background centred in the fit window. These correction terms are essential, considering the large number of counts in the peaks. We treat the DEP and SEP regions independently, representing the 'echo' peak by the same function, with its shape parameters determined by the immediately adjacent peak, and its energy fixed to 10.6 keV above the escape peak energy. The branching ratio B determines the number of counts in the echo peak, relative to each escape peak. This approach improves over the assumption of a flat background made in ref. 36, where the upper limit was computed from a single bin with width 2.8 σ in the echo region, which can bias the result if some curvature is present.

In both escape regions, the data are consistent with a branching ratio of zero. In the SEP region a non-zero best-fit value is preferred, though its lower limit is still statistically consistent with zero signal (<1σ significance). While the DEP region alone provides the most restrictive limit (at 90% CL), the same physical process applies to both the DEP and SEP, and we report the combined result as our primary limit, $\beta^2/2 < 3.69\times10^{-4}$ (90% CL). This is currently the most stringent limit from an atomic Type I PEP violation search, improving the previous best limit by ~70% (ref. 36).

Table 1 gives exclusion limits for each region, and the peak-shape parameters and profile likelihood scan results are given in Extended Data Table 1 and Extended Data Fig. 1.

Type III PEP violation test with low-energy data

We also searched for Type III PEP-violating transition of an L-shell electron in a Ge atom to the already occupied K shell[10,15], shown in Fig. 1. The signature of this process is a Gaussian peak at 10.6 keV, which would appear as a shoulder on the 10.37 keV ^{68}Ge peak. Similar to the charge non-conservation (CNC) search, we search for the PEP-violating atomic transition with the 37.5 kg yr low-energy dataset. The total efficiency of the low-energy cuts is (91 ± 2)% at 10.6 keV, and we set an upper limit on the count rate in the spectrum at the region of interest with the same profile likelihood technique.

We find an upper limit on the count rate at 10.6 keV, $R = 0.0041$ counts per kg d (90% CL), shown in Fig. 5. We then find the mean lifetime, $\tau_e = n_{Ge}/R = 1.66\times10^{32}$ s (90% CL). MAJORANA previously set the most stringent upper limit at 90% CL on this atomic Type III process, at $\beta^2/2 < 8.5\times10^{-48}$ with 478 kg d exposure[15]. Comparing to the 1.7×10^{-16} s mean lifetime of a standard K–α transition in Ge, we set an improved limit on the PEP-violating transition at $\beta^2/2 < 1.03\times10^{-48}$ (90% CL), a factor 8.3 improvement over the previous limit[15].

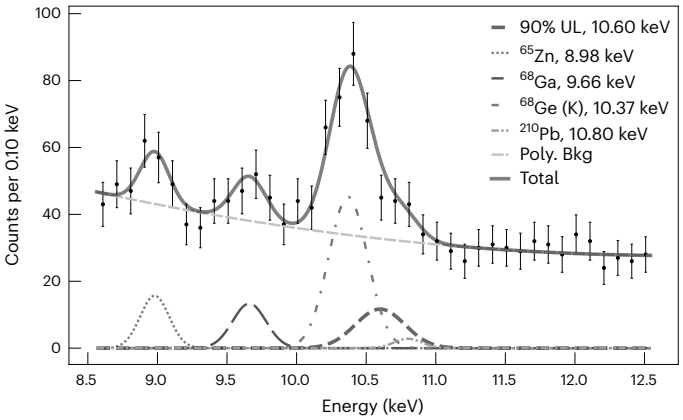

Fig. 5 | A PEP-violating transition of an L-shell electron to the fully occupied K shell in Ge would produce a peak at 10.6 keV. This signature was not observed in the DEMONSTRATOR dataset, and an upper limit on the rate is set, $R = 0.0041$ counts per kg d (90% CL). Error bars are Poisson distributed, and the y axis is given in counts per 0.1 keV bin. As before, data is fit to a polynomial function with expected background lines from ^{65}Zn, ^{68}Ga, ^{68}Ge and ^{210}Pb.

Discussion

Low-background underground radiation detectors offer a unique environment to search for weak signatures from non-standard processes. The large datasets collected by MAJORANA allowed significant improvements in each search above existing limits; the CNC result is the best for ($e \rightarrow$ invisibles) since the 1999 DAMA result. This search based on atomic transitions is an important complement to nucleon-based searches such as Borexino[41], as well as other atomic searches for PEP violation such as VIP-2 (refs. 37,38). Larger Ge arrays with lower backgrounds are currently in active development[44] and an order-of-magnitude improvement in these tests of fundamental quantum mechanical principles may soon be attained.

Online content

Any methods, additional references, Nature Portfolio reporting summaries, source data, extended data, supplementary information, acknowledgements, peer review information; details of author contributions and competing interests; and statements of data and code availability are available at https://doi.org/10.1038/s41567-024-02437-9.

References

1. Wu, C. S., Ambler, E., Hayward, R. W., Hoppes, D. D. & Hudson, R. P. Experimental test of parity conservation in beta decay. *Phys. Rev.* **105**, 1413–1415 (1957).
2. Freedman, S. & Clauser, J. Experimental test of local hidden-variable theories. *Phys. Rev. Lett.* **28**, 938–941 (1972).
3. Aspect, A., Dalibard, J. & Roger, G. Experimental test of Bell's inequalities using time-varying analyzers. *Phys. Rev. Lett.* **49**, 1804–1807 (1982).
4. Bouwmeester, D. et al. Experimental quantum teleportation. *Nature* **390**, 575–579 (1997).
5. Ignatiev, A. & Kuzmin, V. Search for slight violations of the Pauli principle. *JETP Lett.* **47**, 6–8 (1987).
6. Greenberg, O. W. & Mohapatra, R. N. Local quantum field theory of possible violation of the Pauli principle. *Phys. Rev. Lett.* **59**, 2507–2510 (1987).
7. Greenberg, O. Particles with small violations of Fermi or Bose statistics. *Phys. Rev. D* **43**, 4111–4120 (1991).
8. Greenberg, O. Theories of violation of statistics. *AIP Conf. Proc.* **545**, 113–127 (2000).

9. Bernabei, R. et al. New search for processes violating the Pauli exclusion principle in sodium and in iodine. *Eur. Phys. J. C* **62**, 327–332 (2009).
10. Abgrall, N. et al. Search for Pauli exclusion principle violating atomic transitions and electron decay with a p-type point contact germanium detector. *Eur. Phys. J. C* **76**, 619 (2016).
11. Okun, L. & Zeldovich, Y. Paradoxes of unstable electron. *Phys. Lett. B* **78**, 597–600 (1978).
12. Mohapatra, R. Possible nonconservation of electric charge. *Phys. Rev. Lett.* **59**, 1510–1512 (1987).
13. Aalseth, C. et al. Search for neutrinoless double-β decay in ^{76}Ge with the MAJORANA DEMONSTRATOR. *Phys. Rev. Lett.* **120**, 132502 (2018).
14. Arnquist, I. et al. Final result of the MAJORANA DEMONSTRATOR's search for neutrinoless double-β decay in ^{76}Ge. *Phys. Rev. Lett.* **130**, 062501 (2023).
15. Abgrall, N. et al. New limits on bosonic dark matter, solar axions, Pauli exclusion principle violation, and electron decay from the MAJORANA DEMONSTRATOR. *Phys. Rev. Lett.* **118**, 161801 (2017).
16. Arnquist, I. et al. Exotic dark matter search with the MAJORANA DEMONSTRATOR. *Phys. Rev. Lett.* **132**, 041001 (2024).
17. Alvis, S. et al. First limit on the direct detection of lightly ionizing particles for electric charge as low as e/1000 with the MAJORANA DEMONSTRATOR. *Phys. Rev. Lett.* **120**, 211804 (2018).
18. Alvis, S. et al. Search for trinucleon decay in the MAJORANA DEMONSTRATOR. *Phys. Rev. D* **99**, 072004 (2019).
19. Arnquist, I. et al. Search for spontaneous radiation from wave function collapse in the MAJORANA DEMONSTRATOR. *Phys. Rev. Lett.* **129**, 080401 (2022).
20. Workman, R. Particle Data Group. *Prog. Theor. Exp. Phys.* **2022**, 083C01 (2022).
21. Belli, P. et al. New experimental limit on the electron stability and non-Paulian transitions in iodine atoms. *Phys. Lett. B* **460**, 236–241 (1999).
22. Witten, E. Symmetry and emergence. *Nat. Phys.* **14**, 116–119 (2018).
23. Chu, S. Gauge-invariant charge nonconserving processes and the solar neutrino puzzle. *Mod. Phys. Lett. A* **11**, 2251–2257 (1996).
24. Ignatiev, A., Kuzmin, V. & Shaposhnikov, M. Is the electric charge conserved? *Phys. Lett. B* **84**, 315–318 (1979).
25. Dubovsky, S., Rubakov, V. & Tinyakov, P. Is the electric charge conserved in brane world? *J. High Energy Phys.* **2000**, 041 (2000).
26. Agostini, M. et al. Test of electric charge conservation with Borexino. *Phys. Rev. Lett.* **115**, 231802 (2015).
27. Pauli, W. On the connexion between the completion of electron groups in an atom with the complex structure of spectra. *Zeitschrift für Physik* **31**, 765–783 (1925).
28. Weinberg, S. Feynman rules for any spin. *Phys. Rev.* **133**, B1318–B1332 (1964).
29. Suzuki, Y. et al. Study of invisible nucleon decay, $n \to \nu\nu\nu$, and a forbidden nuclear transition in the Kamiokande detector. *Phys. Lett. B* **311**, 357–361 (1993).
30. Bernabei, R. et al. Search for non-Paulian transitions in ^{23}Na and ^{127}I. *Phys. Lett. B* **408**, 439–444 (1997).
31. Curceanu, C. et al. Test of the Pauli exclusion principle in the VIP-2 underground experiment. *Entropy* **19**, 300 (2017).
32. Messiah, A. & Greenberg, O. Symmetrization postulate and its experimental foundation. *Phys. Rev.* **136**, B248–B267 (1964).
33. Greenberg, O. & Mohapatra, R. Phenomenology of small violations of Fermi and Bose statistics. *Phys. Rev. D* **39**, 2032–2038 (1989).
34. Akama, K., Terazawa, H. & Yasuè, M. Superficial violation of the Pauli principle due to the possible substructure of electrons. *Phys. Rev. Lett.* **68**, 1826–1829 (1992).
35. Addazi, A. & Marcianò, A. A modern guide to θ-Poincaré. *Int. J. Mod. Phys. A* **35**, 2042003 (2020).
36. Elliott, S., LaRoque, B., Gehman, V., Kidd, M. & Chen, M. An improved limit on Pauli-exclusion-principle forbidden atomic transitions. *Found. Phys.* **42**, 1015–1030 (2012).
37. Piscicchia, K. et al. VIP-2—high-sensitivity tests on the Pauli exclusion principle for electrons. *Entropy* **22**, 1195 (2020).
38. Napolitano, F. et al. Testing the Pauli exclusion principle with the VIP-2 experiment. *Symmetry* **14**, 893 (2022).
39. Thoma, M. & Nolte, E. Limits on small violations of the Pauli exclusion principle in the primordial nucleosynthesis. *Phys. Lett. B* **291**, 484–487 (1992).
40. Nolte, E. et al. Accelerator mass spectrometry for tests of the Pauli exclusion principle and for detection of beta beta decay products. *J. Phys. G* **17**, S355–S362 (1991).
41. Bellini, G. et al. New experimental limits on the Pauli-forbidden transitions in ^{12}C nuclei obtained with 485 days Borexino data. *Phys. Rev. C* **81**, 034317 (2010).
42. Alvis, S. et al. Search for neutrinoless double-β decay in ^{76}Ge with 26 kg-yr of exposure from the MAJORANA DEMONSTRATOR. *Phys. Rev. C* **100**, 025501 (2019).
43. Arnquist, I. et al. Energy calibration of germanium detectors for the MAJORANA DEMONSTRATOR. *J. Instrum.* **18**, P09023 (2023).
44. Abgrall, N. et al. LEGEND-1000 preconceptual design report. Preprint at https://arxiv.org/abs/2107.11462 (2021).

The MAJORANA Collaboration

I. J. Arnquist[1], F. T. Avignone III[2,3], A. S. Barabash[4], C. J. Barton[5,22], K. H. Bhimani[6,7], E. Blalock[7,8], B. Bos[6,7], M. Busch[7,9], M. Buuck[10], T. S. Caldwell[6], Y-D. Chan[11], C. D. Christofferson[12], P.-H. Chu[13], M. L. Clark[6,7], C. Cuesta[14], J. A. Detwiler[10], Yu. Efremenko[3,15], H. Ejiri[16], S. R. Elliott[13], G. K. Giovanetti[17], M. P. Green[3,7,8], J. Gruszko[6,7], I. S. Guinn[3], V. E. Guiseppe[3], C. R. Haufe[6,7], R. Henning[6,7], D. Hervas Aguilar[6,7], E. W. Hoppe[1], A. Hostiuc[10], M. F. Kidd[18], I. Kim[13,23] ✉, R. T. Kouzes[1], T. E. Lannen V[2], A. Li[6,7,24], J. M. López-Castaño[3], E. L. Martin[6,7,25], R. D. Martin[19], R. Massarczyk[13], S. J. Meijer[13], T. K. Oli[5,26], L. S. Paudel[5], W. Pettus[20], A. W. P. Poon[11], D. C. Radford[3], A. L. Reine[6,7], K. Rielage[13], N. W. Ruof[10,23], D. C. Schaper[13], D. Tedeschi[2], R. L. Varner[3], S. Vasilyev[21], J. F. Wilkerson[3,6,7], C. Wiseman[10] ✉, W. Xu[5], C.-H. Yu[3] & B. X. Zhu[13,27]

[1]Pacific Northwest National Laboratory, Richland, WA, USA. [2]Department of Physics and Astronomy, University of South Carolina, Columbia, SC, USA. [3]Oak Ridge National Laboratory, Oak Ridge, TN, USA. [4]National Research Center "Kurchatov Institute" Institute for Theoretical and Experimental

Physics, Moscow, Russia. [5]Department of Physics, University of South Dakota, Vermillion, SD, USA. [6]Department of Physics and Astronomy, University of North Carolina, Chapel Hill, NC, USA. [7]Triangle Universities Nuclear Laboratory, Durham, NC, USA. [8]Department of Physics, North Carolina State University, Raleigh, NC, USA. [9]Department of Physics, Duke University, Durham, NC, USA. [10]Center for Experimental Nuclear Physics and Astrophysics, and Department of Physics, University of Washington, Seattle, WA, USA. [11]Nuclear Science Division, Lawrence Berkeley National Laboratory, Berkeley, CA, USA. [12]South Dakota Mines, Rapid City, SD, USA. [13]Los Alamos National Laboratory, Los Alamos, NM, USA. [14]Centro de Investigaciones Energéticas, Medioambientales y Tecnológicas, CIEMAT 28040, Madrid, Spain. [15]Department of Physics and Astronomy, University of Tennessee, Knoxville, TN, USA. [16]Research Center for Nuclear Physics, Osaka University, Ibaraki, Japan. [17]Physics Department, Williams College, Williamstown, MA, USA. [18]Tennessee Tech University, Cookeville, TN, USA. [19]Department of Physics, Engineering Physics and Astronomy, Queen's University, Kingston, Ontario, Canada. [20]IU Center for Exploration of Energy and Matter, and Department of Physics, Indiana University, Bloomington, IN, USA. [21]Joint Institute for Nuclear Research, Dubna, Russia. [22]Present address: Roma Tre University and INFN Roma Tre, Rome, Italy. [23]Present address: Lawrence Livermore National Laboratory, Livermore, CA, USA. [24]Present address: University of California San Diego, La Jolla, CA, US. [25]Present address: Duke University, Durham, NC, USA. [26]Present address: Argonne National Laboratory, Lemont, IL, USA. [27]Present address: Jet Propulsion Laboratory, California Institute of Technology, Pasadena, CA, USA.
✉e-mail: inwookkim.physics@gmail.com; wisecg@uw.edu

Methods

Detectors and data-taking scheme

The DEMONSTRATOR was located at the 4,850 ft underground of the Sanford Underground Research Facility in Lead, South Dakota, consisting of two separate ultra-low-background modules of p-type point contact HPGe detectors with a total mass of 44.1 kg, of which 29.7 kg were enriched to 88% in ^{76}Ge (ref. 45). The detectors were operated in a vacuum cryostat within a graded shield made from ultra-low-background electroformed Cu and other shielding materials sourced to meet stringent material purity requirements[46].

The DEMONSTRATOR calibration system accommodates a ^{228}Th line source through a track penetrating the shield and surrounding each cryostat in a helical shape[47]. When deployed, the line source exposed all detectors in the array for energy calibration and stability determination. During normal operations, sources were deployed weekly for 60–90 min to perform routine energy calibrations, while longer runs (12–24 h) were taken to refine energy and other pulse shape analysis parameters.

From 2015–2019 the original set of 35 ^{enr}Ge detectors were operated, using a data blindness scheme alternating 31 h of open data followed by 93 h of blinded data, to mitigate possible bias in the development of analysis routines. Analysis of the calibration dataset does not employ a blinded approach. The DEMONSTRATOR continues to operate with 14.3 kg of natural Ge detectors in a single module for background studies and other rare-event searches.

Peak fits at low energy

The peak scanning algorithm uses a $\pm(7\sigma_{\rm res}+1)$ keV window near the peak position as the fit region of interest (ROI), where $\sigma_{\rm res}$ is the exposure-weighted combined detector resolution as a function of energy. The 1 keV offset ensures an ROI of at least 2 keV, even for a vanishingly small σ. The ROI for the PEP-violating transition search at 10.6 keV is 8.6–12.6 keV, and the ROI for the charge non-conserving electron decay at 11.1 keV is 9.1–13.2 keV. In the low-energy background data near the 10.6 keV signature, cosmogenic peaks at ^{65}Zn (8.98 keV), ^{68}Ga (9.66 keV), and ^{68}Ge (10.37 keV) are expected. External ^{210}Pb may also induce a peak at 10.8 keV. The energy calibration in the low-energy region is precise enough to treat the location of the cosmogenic peaks as fixed at the literature values. Other contributions from tritium beta decay and Compton scattering from higher energy peaks form a background continuum that is separable from the peak-like signature, and is approximated by a second-order polynomial within the ROIs.

In the narrow ROIs where the background continuum can be approximated as a second-order polynomial, the spectrum is modelled as

$$\mathcal{P}(E;\boldsymbol{\theta}) = \eta(E)\left(n_0\mathcal{P}_{\rm poly} + \sum_i^{n_{\rm pks}} n_i\,\mathcal{P}_{G,i} + n_{\rm obs}\mathcal{P}_{\rm rare}\right), \tag{1}$$

where $\mathcal{P}_{\rm poly}$, $\mathcal{P}_{G,i}$ and $\mathcal{P}_{\rm rare}$ are the normalized spectral distributions for the polynomial background as a function of energy E, i-th cosmogenic peak and the rare-event peak of interest, respectively, and n_0, n_i and $n_{\rm obs}$ are the number of events in each distribution. Additional nuisance parameters are denoted $\boldsymbol{\theta}$. We fit the model spectrum to the data using the unbinned extended likelihood method[48–50]. While the shape parameters for the polynomial background are unbounded, the widths of the Gaussian rare peak and background peaks are constrained by the detector energy resolution. Profiling the likelihood function by varying the number of counts in the rare signal peak and re-fitting the nuisance parameters at each step is the standard technique which results in a conservative upper limit on the rate. The signal peaks in both the CNC and Type III PEP searches overlap to some extent with the cosmogenic lines. The likelihood contour is typically flat up to the number of counts assigned to the overlapping peaks, and only increases to the desired CL above these counts; hence the presence of overlapping peaks does not result in an artificially better limit. Figure 5 shows the spectral fit in the ROI of the PEP-violating atomic transition in Ge at the 90% CL upper limit.

The total acceptance efficiency $\eta(E)$ of the low-energy data cleaning cuts is determined by convolving the data cleaning efficiency, the individual detector threshold efficiencies, and the efficiency of the energy-degraded slow pulse event rejection[51]. The low-energy cuts retain (91 ± 2)% of single-site events in our ROI, which we take to be constant within each narrow-fit window. We note that the efficiency correction is a smooth function and will not introduce peak structures, and remains above 80% acceptance down to 3 keV (ref. 16). Complementary searches for other PEP-violating atomic transitions, including jumps to the L shell (~1.3 keV) and other between-shell jumps, are possible in principle. However, in the DEMONSTRATOR'S energy spectrum, the L-shell peak is not resolvable from the background and in a region of steeply dropping acceptance efficiency close to the analysis energy lower limit.

Peak fits at high energy

Our search for the PEP-violating 'echo' peaks, located 10.6 keV above the SEP and DEP, utilizes a standard binned profile likelihood analysis, implemented with the iminuit toolkit[52]. We perform a fit to our signal model using the ExtendedBinnedNLL cost function. The two peak regions are fit independently, since the parameters of each echo peak are strongly constrained by the adjacent large-amplitude escape peak. The number of counts in the echo peak is determined by the product of the number of counts in the escape peak times the branching ratio B, which is equal to the PEP-violating parameter $\beta^2/2$. If its best-fit value is not statistically significant (consistent with $B=0$), we report upper limits on B by profiling over the likelihood function.

A recent report from MAJORANA[43] gives a detailed model of the composition of the germanium peak shape as a function of energy, including several features which are only observable at the large counting statistics available to the full Majorana calibration dataset. The energy regions selected are chosen where the Compton background can be accurately modelled by a quadratic term, avoiding a nearby gamma peak from ^{212}Bi at 1,620 keV. The peak-shape function is a sum of a Gaussian with several correction terms, given by

$$\mathcal{P}(E) = \mathcal{G}(E) + \mathcal{T}_{\rm HE}(E) + \mathcal{T}_{\rm LE}(E) + \mathcal{S}(E). \tag{2}$$

The normalized Gaussian function $G(E)$ includes the full number of counts A attributable to the peak, the mean energy μ and width σ, and the fractional counts attributable to the low- and high-energy tails $T_{\rm HE}$ and $T_{\rm LE}$, given by $f_{\rm l}$ and $f_{\rm h}$:

$$\mathcal{G}(E) = \frac{A(1-f_{\rm l}-f_{\rm h})}{\sqrt{2\pi}\sigma}\exp\left(\frac{-(E-\mu)^2}{2\sigma^2}\right). \tag{3}$$

Both the high- and low-energy tails are described by an exponentially modified Gaussian function

$$\mathcal{T}_\alpha(E) = \frac{Af_\alpha}{2\gamma_\alpha}\exp\left(\frac{\sigma^2}{2\gamma_\alpha^2}\pm\frac{E-\mu}{\gamma_\alpha}\right) \times \mathrm{erfc}\left(\frac{\sigma}{\sqrt{2}\gamma_\alpha}\pm\frac{E-\mu}{\sqrt{2}\sigma}\right). \tag{4}$$

Here, the index $\alpha=\pm1$ corresponds to the $\pm$ sign choice of high-(low-)energy tail, and $\gamma_{\rm l}$, $\gamma_{\rm h}$ the corresponding decay constant. A smoothed step function $S(E)$ with fractional height H is included to account for events which have undergone small-angle Compton scattering, and not contributing directly to the main peak. It is defined in terms of the complementary error function (erfc). It can be positive for incoming gammas, and negative for outgoing gammas.

$$\mathcal{S}(E) = \frac{AH}{2}\mathrm{erfc}\left(\frac{E-\mu}{\sqrt{2}\sigma}\right). \tag{5}$$

Finally, the background function $\mathcal{B}(E)$ is modelled by a second-order sum of Legendre polynomials ($P_{1,2}$) centred in the fit region is used to describe the background in the escape and echo peak regions, using three free parameters a_0, a_1 and a_2. The fit window is defined between low and high energies $E_{\rm lo}$ and $E_{\rm hi}$, with the center at $E_{\rm cen}$.

$$\mathcal{B}(E) = a_0 + a_1 P_1(E - E_{\mathrm{cen}}) + a_2 P_2(E - E_{\mathrm{cen}}). \quad (6)$$

Centring the terms in the fit region ($E_{\mathrm{cen}} = (E_{\mathrm{hi}} - E_{\mathrm{lo}})/2$) avoids correlations in the fit parameters and ensures a more stable fit for all values of the branching ratio B.

The full signal model $\mathcal{M}$ consists of contributions from the two peaks and the background term

$$\begin{aligned}\mathcal{M}(E) = {} & \mathcal{P}(E, A, \mu, \boldsymbol{\theta}) \\ & + \mathcal{P}(E, BA, \mu + 10.6\mathrm{keV}, \boldsymbol{\theta}) \\ & + \mathcal{B}(E, a_0, a_1, a_2, E_{\mathrm{lo}}, E_{\mathrm{hi}}).\end{aligned} \quad (7)$$

The nuisance parameters common to both peaks are given by

$$\boldsymbol{\theta} = (\sigma, f_{\mathrm{l}}, f_{\mathrm{h}}, \gamma_{\mathrm{l}}, \gamma_{\mathrm{h}}, H). \quad (8)$$

To ensure a robust fit, initial guesses for A, μ, σ, H, and so on are numerically estimated from the histogram, and a least-squares fit to the escape peak and background is performed. Using these results, the echo peak is included in a full likelihood fit to obtain the best-fit values for all parameters, including the branching ratio B. Extended Data Table 1 gives the best-fit results and corresponding uncertainties on all parameters from each fit.

Following the best-fit step, a profile of the likelihood function was run using the MINOS algorithm in iminuit, for the DEP and SEP search regions. Results from this scan are shown in Extended Data Fig. 1. While the best-fit for the DEP region is consistent with zero, the single-escape region prefers a non-zero best-fit value. Nonetheless, the lower limit in the SEP region does not exceed 1σ significance, and we report the upper limit on B in both cases. Adding the two likelihood curves, and computing the change in $\Delta\chi^2$ to the desired significance level, we see that the DEP result is the most restrictive at the 90% CL, while the combined result is more restrictive at 99.7% CL. However, since the same underlying physical process contributes to both regions equally, we quote the combined upper limit on B (and hence $\beta^2/2$) as the primary result.

Alternate analysis schemes exploiting the close-packed detector arrangement of the DEMONSTRATOR were also considered, including a technique of selecting only calibration events (multidetector hits) where one detector records a 511 keV energy deposition, and searching for the same 'echo' peak signatures. For the Majorana dataset, estimates indicate this method increases the signal-to-background (S/B) of the peaks by ~15% but lowers the overall number of events available for analysis by 66%. Near the SEP, we would require 1,000 times more calibration data to make this method competitive, and the DEP requires another factor of 100 increase in statistics to provide similar results as the primary scheme which considers all available events.

Data availability

Source data are provided with this paper.

Code availability

The analysis codes are available from the corresponding authors on reasonable request.

References

45. Abgrall, N. et al. The MAJORANA DEMONSTRATOR neutrinoless double-beta decay experiment. *Adv. High Energy Phys.* **2014**, 365432 (2014).
46. Abgrall, N. et al. The MAJORANA DEMONSTRATOR radioassay program. *Nucl. Instrum. Methods Phys. Res. A* **828**, 22–36 (2016).
47. Abgrall, N. et al. The MAJORANA DEMONSTRATOR calibration system. *Nucl. Instrum. Methods Phys. Res. A* **872**, 16–22 (2017).
48. Wilks, S. The large-sample distribution of the likelihood ratio for testing composite hypotheses. *Ann. Math. Stat.* **9**, 60–62 (1938).
49. Rolke, W., López, A. & Conrad, J. Limits and confidence intervals in the presence of nuisance parameters. *Nucl. Instrum. Methods Phys. Res. A* **551**, 493–503 (2005).
50. James, F. *Statistical Methods in Experimental Physics* (World Scientific Publishing Company, 2006).
51. Wiseman, C. A low energy rare event search with the MAJORANA DEMONSTRATOR. *J. Phys. Conf. Ser.* **1468**, 012040 (2020).
52. Dembinski, H. et al. scikit-hep/iminuit (v2.24.0). *Zenodo* https://doi.org/10.5281/zenodo.8249703 (2023).

Acknowledgements

This material is based upon work supported by the US Department of Energy, Office of Science, Office of Nuclear Physics under contract/award numbers DE-AC02-05CH11231, DE-AC05-00OR22725, DE-AC05-76RL0130, DE-FG02-97ER41020, DE-FG02-97ER41033, DE-FG02-97ER41041, DE-SC0012612, DE-SC0014445, DE-SC0018060, DE-SC0022339 and LANLEM77/LANLEM78. We acknowledge support from the Particle Astrophysics Program and Nuclear Physics Program of the National Science Foundation through grant numbers MRI-0923142, PHY-1003399, PHY-1102292, PHY-1206314, PHY-1614611, PHY-1812409, PHY-1812356, PHY-2111140 and PHY-2209530. We gratefully acknowledge the support of the Laboratory Directed Research & Development (LDRD) programme at Lawrence Berkeley National Laboratory for this work. We gratefully acknowledge the support of the US Department of Energy through the Los Alamos National Laboratory LDRD Program, the Oak Ridge National Laboratory LDRD Program and the Pacific Northwest National Laboratory LDRD Program for this work. We gratefully acknowledge the support of the South Dakota Board of Regents Competitive Research Grant. We acknowledge the support of the Natural Sciences and Engineering Research Council of Canada, funding reference number SAPIN-2017-00023, and from the Canada Foundation for Innovation John R. Evans Leaders Fund. We acknowledge support from the 2020/2021 L'Oréal-UNESCO for Women in Science Programme. This research used resources provided by the Oak Ridge Leadership Computing Facility at Oak Ridge National Laboratory and by the National Energy Research Scientific Computing Center, a US Department of Energy Office of Science User Facility. We thank our hosts and colleagues at the Sanford Underground Research Facility for their support.

Author contributions

All authors were involved in various aspects of detector construction, operation, maintenance, data acquisition, data-taking shifts, software development, data processing and analysis. C.W. and I.K. developed the low-energy data cleaning, and low-energy statistical analysis and spectrum fit techniques. J.M.L.-C. and C.W. conducted the high-energy spectral analysis and derived the limit on the Type I PEP-violating process. I.K. derived limits for the electron lifetime and Type III PEP-violating process. C.W. and I.K. wrote the paper. All authors reviewed, commented and approved the results and the final version of the paper.

Competing interests

The authors declare no competing interests.

Additional information

Extended data is available for this paper at https://doi.org/10.1038/s41567-024-02437-9.

Correspondence and requests for materials should be addressed to I. Kim or C. Wiseman.

Peer review information *Nature Physics* thanks Miriam Diamond, Ziqing Hong, Rabindra Mohapatra and Alessio Porcelli for their contribution to the peer review of this work.

https://doi.org/10.1038/s41567-024-02437-9

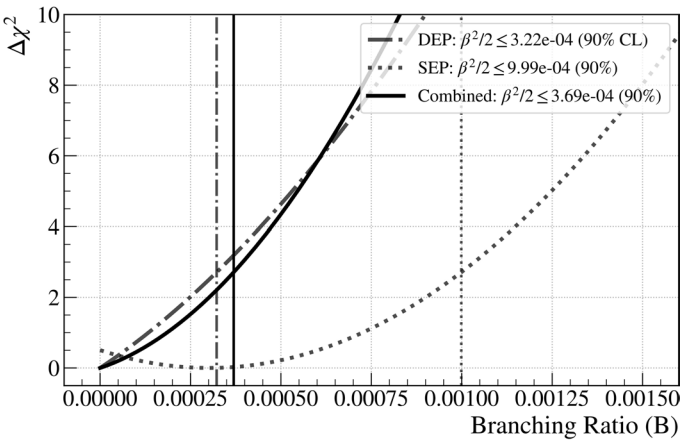

Extended Data Fig. 1 | Profiles of the likelihood function over the branching ratio $B = \beta^2/2$, defined as the ratio of lifetimes between PEP-obeying and PEP-violating atomic transitions of electrons. DEP: $\beta^2/2 \leq 3.22e{-}04$ (90% CL). SEP: $\beta^2/2 \leq 9.99e{-}04$ (90%). Combined: $\beta^2/2 \leq 3.69e-04$ (90%). The profiles from the single-escape peak region (dotted) and the double-escape peak region (dot-dashed) are added and shifted to produce the combined curve (solid black). The upper limits are computed at the intersection $\Delta\chi^2 = 2.71$, representing the 90% confidence level. Vertical lines representing the 90% upper limits are added for reference.

https://doi.org/10.1038/s41567-024-02437-9

Extended Data Table 1 | Best-fit parameters for the germanium peak shape function in the single-escape peak (SEP) and double-escape peak (DEP) regions

	DEP	SEP
B	$(7.0 \times 10^{-13})^{+1.3\times10^{-4}}_{-7.0\times10^{-13}}$	$(3.0 \times 10^{-4})^{+4.2\times10^{-4}}_{-3.0\times10^{-4}}$
A	$1{,}779{,}000\ ^{+6{,}000}_{-5{,}000}$	$2{,}462{,}300\ ^{+3{,}400}_{-3{,}400}$
μ	$1592.661\ ^{+0.005}_{-0.005}$	$2103.618\ ^{+0.010}_{-0.009}$
σ	$0.823\ ^{+0.003}_{-0.003}$	$1.298\ ^{+0.005}_{-0.005}$
f_l	$0.293\ ^{+0.007}_{-0.007}$	$0.302\ ^{+0.012}_{-0.011}$
f_h	$0.032\ ^{+0.004}_{-0.004}$	$0.075\ ^{+0.005}_{-0.004}$
γ_l	$1.050\ ^{+0.040}_{-0.040}$	$1.314\ ^{+0.037}_{-0.035}$
γ_h	$2.060\ ^{+0.370}_{-0.310}$	$1.640\ ^{+0.100}_{-0.090}$
H	$0.001\ ^{+0.002}_{-0.002}$	$0.001\ ^{+0.001}_{-0.001}$
a_0	$67{,}400\ ^{+1{,}100}_{-1{,}200}$	$84{,}300\ ^{+400}_{-400}$
a_1	$4{,}200\ ^{+1{,}800}_{-1{,}800}$	$3{,}900\ ^{+700}_{-700}$
a_2	$-2{,}200\ ^{+800}_{-700}$	$-1{,}400\ ^{+400}_{-400}$
E_{lo}	1585.0	2090.0
E_{hi}	1608.0	2132.0

The branching ratio to the PEP-violating peak B is included, as well as the amplitude (counts) parameter A, the mean energy μ, and the shape parameters $\sigma, f_{l,h}, \gamma_{l,h}, H$, background polynomial coefficents a_i, and fit regions E_{lo}, E_{hi}. Errors are calculated using the MINOS algorithm in `iminuit`[52].